

Thermoacoustic and photoacoustic characterizations of few-layer graphene by pulsed excitations

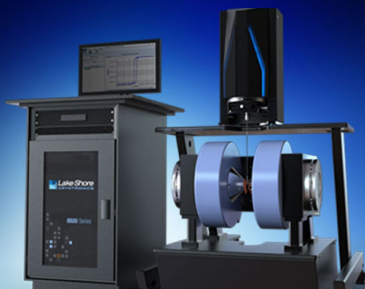
, [Russell S. Witte](#), and [Hao Xin](#)'

Citation: [Appl. Phys. Lett.](#) **108**, 143104 (2016); doi: 10.1063/1.4945661

View online: <http://dx.doi.org/10.1063/1.4945661>


View Table of Contents: <http://aip.scitation.org/toc/apl/108/14>

Published by the [American Institute of Physics](#)



NEW 8600 Series VSM

For fast, highly sensitive
measurement performance

LEARN MORE 

Thermoacoustic and photoacoustic characterizations of few-layer graphene by pulsed excitations

Xiong Wang (王雄),^{1,2,3} Russell S. Witte,² and Hao Xin^{1,a)}

¹Department of Electrical and Computer Engineering, The University of Arizona, Tucson, Arizona 85721, USA

²Department of Medical Imaging, The University of Arizona, Tucson, Arizona 85724, USA

³School of Information Science and Technology, ShanghaiTech University, Shanghai 200031, China

(Received 8 March 2016; accepted 20 March 2016; published online 6 April 2016)

We characterized the thermoacoustic and photoacoustic properties of large-area, few-layer graphene by pulsed microwave and optical excitations. Due to its high electric conductivity and low heat capacity per unit area, graphene lends itself to excellent microwave and optical energy absorption and acoustic signal emanation due to the thermoacoustic effect. When exposed to pulsed microwave or optical radiation, distinct thermoacoustic and photoacoustic signals generated by the few-layer graphene are obtained due to microwave and laser absorption of the graphene, respectively. Clear thermoacoustic and photoacoustic images of large-area graphene sample are achieved. A numerical model is developed and the simulated results are in good accordance with the measured ones. This characterization work may find applications in ultrasound generator and detectors for microwave and optical radiation. It may also become an alternative characterization approach for graphene and other types of two-dimensional materials. © 2016 AIP Publishing LLC.

[<http://dx.doi.org/10.1063/1.4945661>]

As the first discovered two-dimensional (2D) material, graphene has fueled extensive interests in its exciting potential applications propelled by its outstanding thermal, electrical, and mechanical properties.^{1–3} We report thermoacoustic and photoacoustic characterizations of a large-area, few-layer graphene sample with pulsed microwave and optical excitations, respectively. The thermoacoustic effect refers to the excitation of acoustic waves by absorbed electromagnetic energy, delivered by a modulated or pulsed electromagnetic wave, in an electromagnetically lossy sample.^{4–6} For electromagnetic frequencies falling in the optical regime, this effect is named the photoacoustic effect. Such an electromagnetic-to-acoustic energy conversion process is enabled by a concomitant local temperature boost due to energy absorption and thermal expansion in the sample. Thermoacoustic and photoacoustic effects have been most widely applied in biomedical imaging and are referred to as thermoacoustic imaging and photoacoustic imaging, respectively.^{5–14}

Owing to its excellent microwave and optical absorbing capabilities,^{3,15} as well as low heat capacity per unit area,^{16–20} graphene is an excellent thermoacoustic and photoacoustic signal generator.^{17–20} The graphene sample opted in this work contains 2–3 layers, exhibiting enhanced energy absorption compared to monolayer graphene in both the microwave and optical regime.^{21,22} Thermoacoustic and photoacoustic signals unambiguously attributed to the graphene sample were observed. A corresponding numerical model was established to predict the time-domain thermoacoustic signal profile,^{23,24} which exhibited good resemblance with the measurement results. Thermoacoustic and photoacoustic images of the graphene sample were also obtained, which further undoubtedly validates the signals originated from the graphene.

This work is different from the reported works in Refs. 17–20 mainly in two aspects. First, the reported works use sound frequency alternating current applied to the graphene, while the excitation mechanism of the presented characterization work is a remote heating approach by means of pulsed radiation. Second, audible thermoacoustic signals are generated in the reported works, while ultrasonic waves are launched in the current work. In addition, in contrast to the work using oxidized graphene nanoribbons as thermoacoustic and photoacoustic contrast agents,²⁵ this work investigates a large-area graphene sample. This work might provide an alternative perspective to reveal the thermal and mechanical properties of graphene. The applied characterization approaches may serve as a potential fundamental study tool for graphene and other 2D materials.

A schematic description of the thermoacoustic signal generation mechanism is given in Fig. 1(a). Electromagnetic energy delivered by pulsed microwave or optical signals is assimilated by the few-layer graphene. The absorbed energy instantaneously heats up the graphene and the immediately adjacent surrounding materials, i.e., the substrate and coupling liquid touching the graphene.^{26–28} Thermal expansion thereby takes place in the substrate and coupling liquid, which effectively launches thermoacoustic or photoacoustic waves. The resulting ultrasonic waves subsequently propagate to the surrounding environment as illustrated in Fig. 1(a).

Schematic thermoacoustic experimental setup is shown in Fig. 1(b). The sample to be investigated contains 2–3 layers of graphene residing on a 1-mm thick glass substrate.²⁹ The dimensions of the graphene and glass substrate are provided in Fig. 1(c), from which it is seen that the graphene is rectangular with a size of 16 mm × 9 mm while the shape of the substrate is somewhat irregular on one side. The photo of the sample is given in Fig. 1(d). The sheet resistance of the multilayer graphene is about 1000 Ω/sq,³⁰ which is translated to a surface

^{a)}Electronic mail: hxin@email.arizona.edu

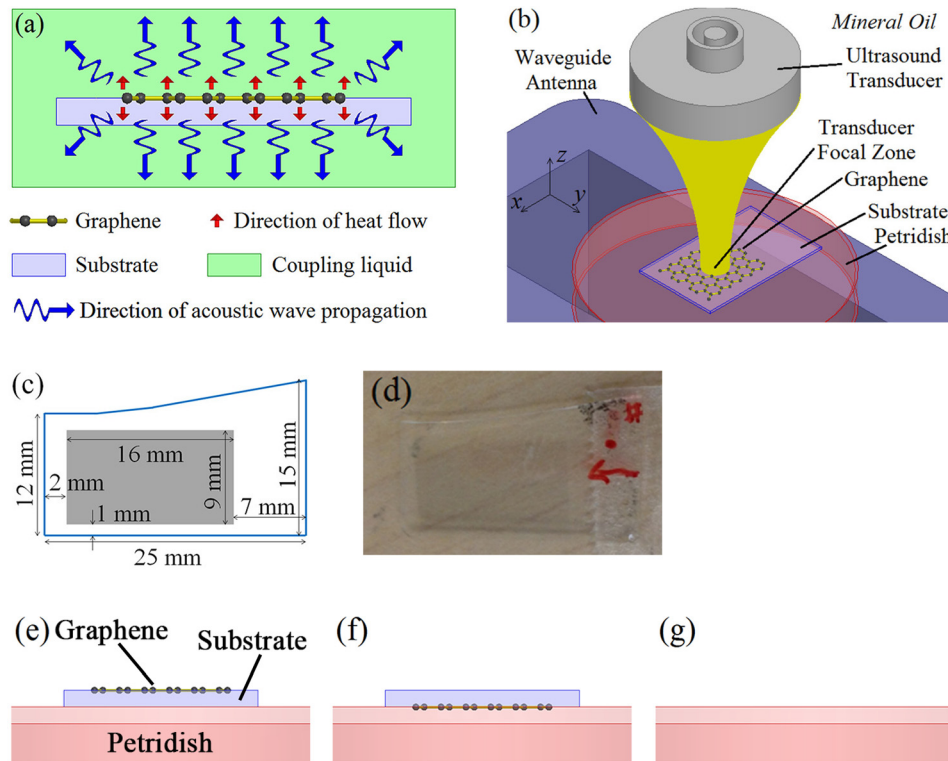


FIG. 1. (a) Side view of a schematic describing the thermoacoustic signal generation mechanism of graphene. (b) Schematic of the experimental setup, in which the employed few-layer graphene is simplified to a single layer graphene. (c) Schematic of the top view of the examined graphene sample. The gray region is the few-layer graphene and the blue line is the boundary of the glass substrate. (d) Photo of the graphene sample. (e)–(g) Side view of the scenarios with graphene on top of the substrate, on bottom of the substrate, and without the sample.

conductivity of 1 mS/sq and classified as a good absorptive material in the microwave frequency band.²¹ The sample was immersed in mineral oil and situated on a petri dish made of polystyrene which acts as a sample holder as sketched in Fig. 1(b). A 1.4 GHz microwave signal from a high power amplifier (117L, Applied Systems Engineering) with 20 kW peak power was modulated by a 1- μ s square pulse. The output of the microwave amplifier fed a rectangular waveguide (WR430 with an aperture dimension of 109.2 mm \times 54.6 mm) antenna,³¹ which radiated the sample from the bottom. The petri dish sat on the flange of the waveguide and the sample was 10 mm above the aperture. A 1-in.-diameter single-element spherically focused ultrasonic transducer (V302, Olympus) centered at 1 MHz was also immersed in the mineral oil to harvest the emanated acoustic signals from the sample. The transducer was mounted on a 3D motorized stage by a cantilever and was scanned in a 5 cm \times 5 cm square region with a step of 1 mm in the xy plane defined in Fig. 1(b). The thermoacoustic signal obtained by the transducer was first amplified by a low-noise amplifier (5072PR, Olympus) with 50 dB gain and then sampled by an oscilloscope (PXI-5922, National Instruments) with a sampling rate of 15 MHz. The signal was also averaged 1000 times to increase the signal-to-noise ratio and the averaged signal was recorded for subsequent data processing.

Thermoacoustic experiments were performed for three different scenarios. First, the sample was arranged so that the graphene was on top of the glass substrate as schematically shown in Fig. 1(e). Second, the sample was flipped over to have the graphene on bottom of the glass substrate (Fig. 1(f)). The third scenario contained no sample except the petri dish (Fig. 1(g)).

Pulse echo ultrasound was first carried out to locate the entire sample in the scanning region for the first two scenarios, and the consequent images are shown in Figs. 2(a) and 2

(b). The shape of the substrate is faithfully recovered in both situations and the areas with graphene are approximately aligned to each other. Measured time-domain thermoacoustic signals for different cases are given in Fig. 2(c), which correspond to the focusing locations of the transducer at P_1 (on the graphene) indicated in Figs. 2(a) and 2(b). Filtering is applied to remove DC components in the signals plotted in Fig. 2(c) to provide a better visibility. A pronounced pulsed ultrasonic signal, with a dominant positive pulse sandwiched by two weaker negative pulses, manifests itself starting around 48 μ s in the time-domain signals acquired when the transducer focuses at P_1 in the graphene region for both the graphene on top (the peak of pulse occurs at 50.1 μ s) and bottom (the peak of pulse occurs at 50.4 μ s) scenarios. The 48 μ s accounts for the acoustic wave propagation time in the mineral oil from the sample to the transducer about 70 mm above. However, for the situations when the transducer focuses on merely the petri dish (the sample is removed) in the third scenario, no thermoacoustic signal is generated in the same time window, implying that the petri dish is lossless and does not induce thermoacoustic signal. The distinction between with/without graphene cases unambiguously demonstrates that the pulse shaped thermoacoustic signals are ascribed to the graphene whose high conductivity and energy absorption capability launch the thermoacoustic effect indirectly in the adjacent substrate and mineral oil. The lossless glass substrate and mineral oil do not directly absorb any microwave energy themselves. Moreover, there is a 0.3 μ s distinguishable time delay between the acoustic pulses for the graphene on top and bottom cases, which represents a 1.1 mm distance offset given the fact that the substrate bears a speed of sound of 3.7 mm/ μ s and corresponds well to the extra acoustic wave propagation time in the 1-mm thick substrate for the graphene on bottom scenario. This further

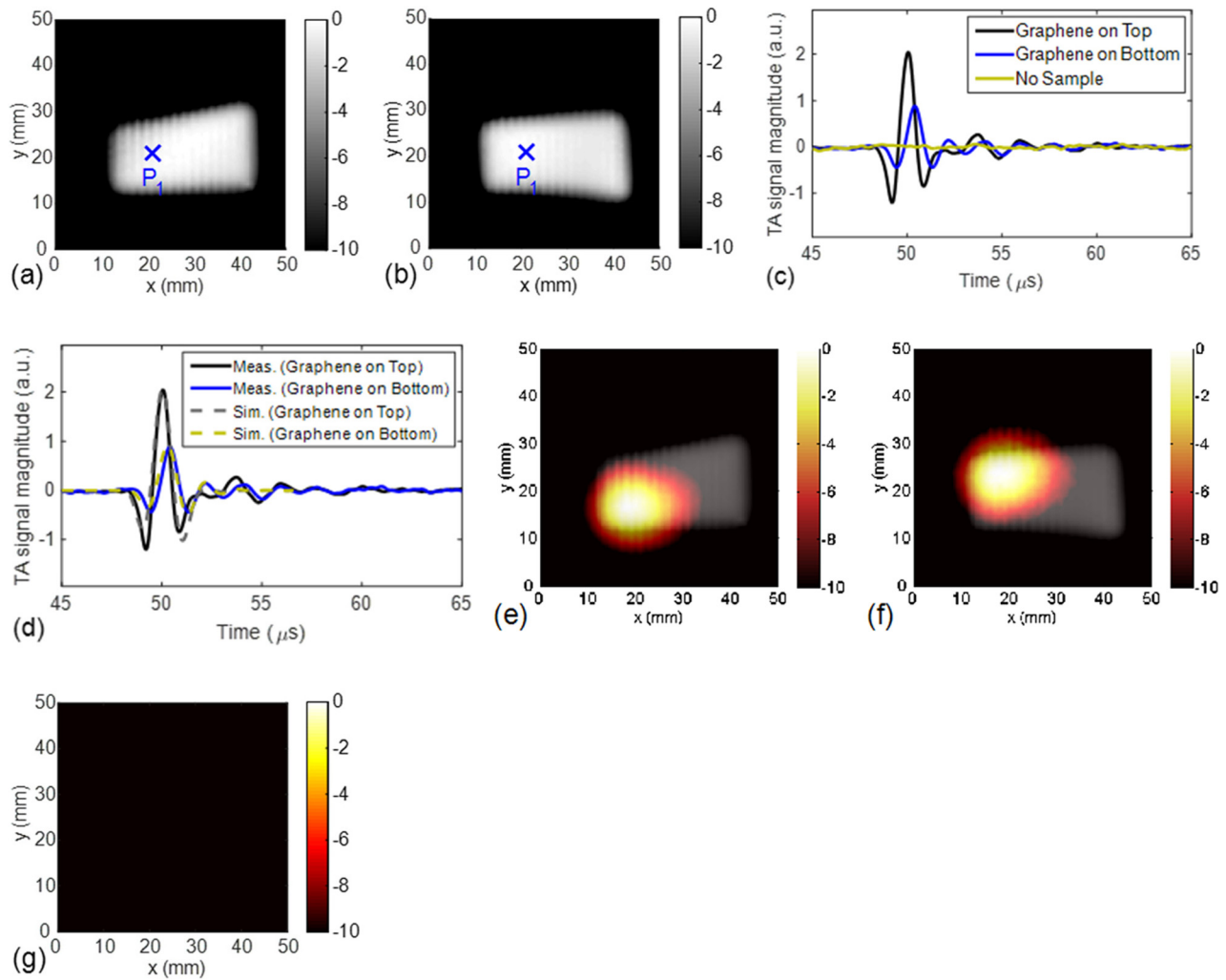


FIG. 2. Experimental results of the thermoacoustic characterization of the graphene sample. (a) and (b) acoustic pulse echo images (in dB scale) for the graphene on top (a) and bottom (b) scenarios. (c) Filtered time-domain thermoacoustic signals for different cases. The focusing location of the transducer is at P_1 defined in (a) and (b). (d) Comparison between normalized measured and simulated time-domain signals. (e)–(g) Thermoacoustic images (hot color in dB scale) for the scenarios with the graphene on top (e), on bottom (f), and without the sample (g). The pulse echo images in (a) and (b) are co-registered with their corresponding thermoacoustic images in (e) and (f) in gray scale, respectively. The magnitude in (e) and (f) are normalized. The scale in (g) is made identical to that in (e).

corroborates the conclusion that the conspicuous pulsed thermoacoustic signals stem from the conducted heat in the vicinity of the graphene. The peak magnitude of the acoustic pulse for the graphene on bottom case is about half of that for the graphene on top case, which is by large measure caused by the acoustic wave reflections in the glass due to acoustic impedance mismatch between the glass and mineral oil.

A corresponding numerical model was developed to provide an auxiliary benchmark to compare with the experimental outcome. Electromagnetic simulations were carried out first to calculate the heat distribution in the sample by a commercial software package High Frequency Structural Simulator (HFSS[®]), in which the sub-nanometer thick graphene can be accurately approximated by a 2D impedance boundary bearing surface resistance of $1000 \Omega/\text{sq}$. Acoustic simulations were done afterwards by MATLAB[®] using the specific absorption rate as the thermoacoustic source to obtain the generated acoustic pressures.^{6,23,24} From the comparison shown in Fig. 2(d), good resemblance is observed in terms of temporal profile of the thermoacoustic pulses,

quantitative magnitude difference in the pulses between the graphene on top and bottom instances, and time delay in the pulses between the two scenarios.

Thermoacoustic images were developed to reconstruct profiles of the heat density distribution in the three scenarios, which are provided in Figs. 2(e)–2(g). For the first two scenarios, the heat density profiles (shown in hot scale) are co-registered with the corresponding pulse echo image of the substrate (depicted in gray scale). The imaging approach has been reported in our previous work.²³ Apparent hot spots appear in the region of graphene in Figs. 2(e) and 2(f), which are associated with the pronounced peaks in the thermoacoustic signals in Fig. 2(c). The reason why elliptical rather than rectangular spots are obtained is because the 4.3-mm-diameter focal spot of the transducer effectively blurs the boundary of the actual heat density distribution in the sample. The relative locations between the high heat density spots and the substrate show good agreement with the structure shown in Figs. 1(c) and 1(d). The dimension of the heat density spot approximately accords with the actual dimension of the rectangular graphene in Fig. 1(c) despite

- ²⁰Y. Tian, H. Tian, Y. L. Wu, L. L. Zhu, L. Q. Tao, W. Zhang, Y. Shu, D. Xie, Y. Yang, Z. Y. Wei, X. H. Lu, T. Ren, C. Shih, and J. Zhao, *Sci. Rep.* **5**, 10582 (2015).
- ²¹B. Wu, H. M. Tuncer, A. Katsounaros, W. Wu, M. T. Cole, K. Ying, L. Zhang, W. I. Milne, and Y. Hao, *Carbon* **77**, 814 (2014).
- ²²C. Casiraghi, A. Hartschuh, E. Lidorikis, H. Qian, H. Harutyunyan, T. Gokus, K. S. Novoselov, and A. C. Ferrari, *Nano Lett.* **7**, 2711 (2007).
- ²³T. Qin, X. Wang, Y. Qin, P. Ingram, G. Wan, R. S. Witte, and H. Xin, *IEEE Antenna Wireless Propag. Lett.* **14**, 1235 (2015).
- ²⁴X. Wang, T. Qin, R. S. Witte, and H. Xin, *IEEE Trans. Microwave Theory Tech.* **63**, 1489 (2015).
- ²⁵G. Lalwani, X. Cai, L. Nie, L. V. Wang, and B. Sitharaman, *Photoacoustics* **1**, 62 (2013).
- ²⁶A. A. Balandin, *Nat. Mater.* **10**, 569 (2011).
- ²⁷K. H. Baloch, N. Voskanyan, M. Bronsgeest, and J. Cumings, *Nat. Nanotechnol.* **7**, 316 (2012).
- ²⁸Z. Wang, R. Xie, C. T. Bui, D. Liu, X. Ni, B. Li, and J. T. L. Thong, *Nano Lett.* **11**, 113 (2011).
- ²⁹Z. Wu, M.S. thesis, The University of Arizona, 2010.
- ³⁰M. Liang, Z. Wu, L. Chen, L. Song, P. Ajayan, and H. Xin, *IEEE Trans. Microwave Theory Tech.* **59**, 2719 (2011).
- ³¹L. Nie, Z. Ou, S. Yang, and D. Xing, *Med. Phys.* **37**, 4193 (2010).